Enhanced Activity for CO Oxidation over Pr- and Cu-Doped CeO 2 Catalysts: Effect of Oxygen Vacancies

ARTICLE *in* THE JOURNAL OF PHYSICAL CHEMISTRY C · AUGUST 2008

Impact Factor: 4.77 · DOI: 10.1021/jp805389k

6 AUTHORS, INCLUDING:

Yunlong Xie
Zhejiang Normal University
34 PUBLICATIONS **509** CITATIONS
SEE PROFILE

Jiqing Lu
Zhejiang Normal University
123 PUBLICATIONS **2,320** CITATIONS
SEE PROFILE

Enhanced Activity for CO Oxidation over Pr- and Cu-Doped CeO_2 Catalysts: Effect of Oxygen Vacancies

Zhi-Ying Pu, Xue-Song Liu, Ai-Ping Jia, Yun-Long Xie, Ji-Qing Lu,* and Meng-Fei Luo*

Zhejiang Key Laboratory for Reactive Chemistry on Solid Surfaces, Institute of Physical Chemistry, Zhejiang Normal University, Jinhua 321004, People's Republic of China

Received: June 19, 2008; Revised Manuscript Received: July 21, 2008

$Ce_{0.9}Pr_{0.1}O_{2-\delta}$, $Ce_{0.95}Cu_{0.05}O_{2-\delta}$, and $Ce_{0.9}Pr_{0.05}Cu_{0.05}O_{2-\delta}$ mixed oxides and pure CeO_2 were prepared with a sol−gel method and were characterized by XRD, in situ Raman, and in situ DRIFTS techniques. The XRD results confirmed the formation of Ce−Pr−O solid solution. The Raman results indicated that a higher concentration of oxygen vacancies was obtained on the Pr-doped samples compared to the $Ce_{0.95}Cu_{0.05}O_{2-\delta}$ and pure CeO_2 samples. Surface chemical states of the $Ce_{0.9}Pr_{0.1}O_{2-\delta}$ and $Ce_{0.9}Pr_{0.05}Cu_{0.05}O_{2-\delta}$ mixed oxides were determined by in situ Raman spectroscopy, which indicated that the surfaces of the two mixed oxides were both close to oxidation state during the reaction, despite of the presence of reducing reactant CO in the gas mixture. The in situ DRIFTS results evidenced the chemisorption of CO in the Cu-containing samples. The catalysts were tested for CO oxidation, and it was found that the enhanced reactivity was closely related to the higher concentrations of the oxygen vacancies and the chemisorbed CO in the catalysts, due to the fact that the oxygen vacancies provide activation centers for O_2 and the Cu^+ ions provide chemisorption sites for CO.

1. Introduction

In recent years, catalytic oxidation of CO has been given much attention due to its wide applications for indoor air cleaning, CO gas sensors, CO_2 lasers, and automotive exhaust treatment.[1,2] Precious-metal catalysts such as Au/TiO_2,[3−5] Au/ZrO_2,[6] and Pt/SnO_2[1,7] have been used for low temperature CO oxidation. However, due to the high price of precious metals, more and more attention has been given to the use of base-metal catalysts, especially copper catalysts.[8−10] Among them, Cu−Ce−O catalysts attract special interest due to their remarkable activities that can even be compared to the noble metals.[11] For example, Liu et al.[12,13] found that the CuO/CeO_2 catalysts exhibited special activities superior to the conventional Cu-based catalysts and these catalysts were as active as Pt catalysts. Our previous work showed that enhanced reactivity could be obtained on the Cu−Ce−O catalysts with high surface areas (>150 m^2 g^{-1}) compared to those with low surface areas (~ 60 m^2 g^{-1}), due to more finely dispersed CuO species and more defects provided by the smaller CeO_2 particles (~ 5 nm).[10,14]

The nature of CO oxidation over Cu−Ce−O catalysts has been widely investigated. Liu et al.[12] conducted a kinetic study of CO oxidation over a CuO/CeO_2 catalyst and found that the reaction rate was proportional to CO partial pressure and independent of O_2 partial pressure in the feed gas. They concluded that the Cu^+ species provided strong CO chemisorption sites, and the reaction occurred at the boundary of $CuO-CeO_2$ interface.[12] Also, a similar conclusion was obtained by the group of Martínez-Arias, based on their DRIFTS study.[15−17] The role of CeO_2 in the catalysts is not only related to its oxygen-storage capacity, but also to its ability to improve dispersion of copper.[18,19] The oxygen mobility in CeO_2 support is important for the catalysts, since the oxygen from the support is available for CO oxidation. Furthermore, the oxygen vacancies are easily formed in the CeO_2 support, and the oxygen vacancies, even in small amounts, seem to favor activity because they provide sites for oxygen activation to form superoxide (O_2^-) species.[20] Fierro et al.[21] confirmed the presence of surface adsorbed O_2^- on a Ce^{4+} site by EPR spectrum. The energy calculation also confirmed that the presence of oxygen vacancies promoted the CO oxidation on the (110) and (310) surfaces of CeO_2.[22] Sedmak et al.[23−25] concluded that the lattice oxygen in the CeO_2 was also involved in the reaction, because the Cu−Ce−O catalyst can catalyze CO oxidation even without the presence of O_2 in the reaction gas.

As mentioned above, it can be seen that the reactivity of $CuO-CeO_2$ catalysts for CO oxidation is influenced by two factors. One is the Cu^+ site for CO chemisorption, and the other is the oxygen vacancy provided by the CeO_2 support, which can in turn generate active oxygen for the reaction. Therefore, one approach to an enhanced CO oxidation activity is to synthesize the CeO_2-based mixed oxide with more oxygen vacancies, which could be achieved by doping it with other rare earth or transition-metal elements, such as Pr[26] and Gd,[27] into the CeO_2 lattice. Particularly, it was pointed out in our previous work that the Pr-doped CeO_2 exhibited a high concentration of oxygen vacancies,[28] which has the potential to be a promising support for oxidative catalysts.

Although oxygen vacancies in $CuO-CeO_2$ catalysts are considered very important to the reaction, they have not yet been studied under reaction conditions. In this work, a series of CeO_2-based mixed oxides doped with Pr and/or Cu were prepared and characterized by various techniques. Surface properties of the samples under the reaction conditions were analyzed with in situ Raman and in situ DRIFT spectroscopies. It could be seen that the reactivity of CO oxidation is remarkably enhanced by the doping of Pr and Cu in the CeO_2. The synergistic role of Pr and Cu doping in the reactivity is also discussed.

* To whom correspondence should be addressed. E-mail: jiqinglu@zjnu.cn, mengfeiluo@zjnu.cn. Fax: +86-579-82282595.

10.1021/jp805389k CCC: $40.75
Published on Web 08/30/2008

2. Experimental Section

2.1. Catalyst Preparation. $Ce_{0.9}Pr_{0.1}O_{2-\delta}$, $Ce_{0.95}Cu_{0.05}O_{2-\delta}$, $Ce_{0.9}Pr_{0.05}Cu_{0.05}O_{2-\delta}$ mixed oxides, and pure CeO_2 were prepared with a sol−gel method, using $Ce(NO_3)_3$ $6H_2O$ (99.9%), $Cu(NO_3)_2$ $3H_2O$ (99.9%), and Pr_6O_{11} (99.9%) as the precursors. For the preparation of $Ce_{0.9}Pr_{0.05}Cu_{0.05}O_{2-\delta}$ catalyst, a certain amount of Pr_6O_{11} was dissolved by the least amount of dense nitric acid required, and a mixed solution of $Ce(NO_3)_3$ and $Cu(NO_3)_2$ was added to form a Ce—Pr—Cu nitrate solution. Then, citric acid with the same molar amount of the cations (Ce + Cu + Pr) was added to the above solution. The mixture was heated at 90 °C under continuous stirring until a viscous gel was obtained. The gel was dried at 120 °C overnight and calcined at 900 °C in air for 4 h with a heating rate of 10 °C min^{-1}. Other catalysts were prepared in a similar manner.

2.2. Characterizations. Specific surface areas (S^{BET}) of the catalysts were calculated from a multipoint Braunauer−Emmett−Teller (BET) analysis of the nitrogen adsorption and desorption isotherms at 77 K recorded on an Autosorb-1 apparatus. The samples were heated at 120 °C in vacuum for 6 h before measurement.

N_2O chemisorption was employed to determine the Cu dispersion of the Cu-containing samples. In a typical measurement, 20 mg of catalyst was placed in a quartz reactor connected to a homemade TPR apparatus, and the sample was heated from room temperature to 500 °C at a heating rate of 10 °C min^{-1}. The amount of H_2 uptake during the reduction was measured by TCD.

The N_2O chemisorption process consists of three sequential steps:

$$CuO + H_2 \rightarrow Cu + H_2O \quad (1)$$

$$2Cu + N_2O \rightarrow Cu_2O + N_2 \quad (2)$$

$$Cu_2O + N_2 \rightarrow 2Cu + H_2O \quad (3)$$

Step 1 represents reduction of CuO in the catalyst. In this step, a flow of H_2 (5%) in N_2 (30 mL min^{-1}) was used as the reducing agent, and the temperature was raised from room temperature to 500 °C with a heating rate of 10 °C min^{-1}. The amount of H_2 consumption (A_1) corresponds to the total amount of CuO in the CuO—CeO_2 catalyst. Step 2 represents oxidation of surface Cu to Cu_2O by N_2O, which is a well-known method to evaluate the dispersion and crystallite size of Cu catalysts.[29] This step was initiated after the reduced catalyst was cooled to 60 °C in He (30 mL min^{-1}) and purged with He for 30 min. Then, pure N_2O (40 mL min^{-1}) was introduced to the catalyst at 60 °C for 1 h. Subsequently, the catalyst was purged with He (30 mL min^{-1}) for 0.5 h to remove the residual N_2O. Step 3 represents reduction of Cu_2O surface species. In this step, a flow of H_2 (5%) in N_2 (30 mL min^{-1}) was also used as the reducing agent, and the temperature was raised from room temperature to 500 °C with a heating rate of 10 °C min^{-1}. The amount of H_2 consumption (A_2) corresponds to 2× of the amount of surface Cu in the CuO—CeO_2 catalyst according to the stoichiometric factor of step 3. The dispersion (D) of CuO, was calculated as follows:

$$D = \frac{2A_2}{A_1} \times 100\% \quad (4)$$

which has been used in literature.[29]

X-ray diffraction (XRD) patterns of the samples were collected on a Philips PW3040/60 automated powder diffractometer equipped with a Philips X'celerator detector using Cu Kα radiation (λ = 0.1542 nm). The working voltage of the instrument was 40 kV, and the working current was 40 mA. The patterns were collected with a 2θ range from 20° to 100°, with a scanning rate of 0.15 ° s^{-1}. Lattice parameters of the samples were calculated by full curve fitting, using Jade 6.5 software.

Raman measurements were performed on a Renishaw RM1000 with a confocal microprobe Raman system using a 514-nm (Ar^+ laser) laser as the excitation source with a dwell time of 20 s, number of scans of 2, and a resolution of 1 cm^{-1}, power of 50%. In situ Raman measurements were performed in a homemade in situ Raman cell linked to the Raman equipment. Gas mixtures used in the in situ measurements were O_2 (1%)−N_2 (99%), O_2 (1%)−CO (1%)−N_2 (98%) and CO (1%)−N_2 (99%). The CO (1%) −N_2 (99%) mixture was deoxygenized before being introduced to the Raman system. In a typical run, about 20 mg of the sample was loaded in the cell and pretreated in O_2 at 400 °C for 1 h and then cooled down to room temperature. Then, the gas mixture was introduced to the cell, and the sample was heated to 500 °C, with a heating rate of 20 °C min^{-1}. Each spectrum was collected after the desired temperature point was held for 30 min. Finally, the sample was cooled to room temperature, and the spectrum was collected again. For the CO—N_2 mixture, after the spectrum was collected, the previous gas was stopped and O_2 was introduced, and the spectrum was collected again.

Diffuse reflectance Infrared Fourier transform (DRIFT) spectra of the samples were recorded using a Nicolet 470 spectrometer equipped with an MCT detector and a DRIFTS cell (Harrick), under reaction conditions with a resolution of 4 cm^{-1}. An accumulation of 32 scans was used for collecting background spectra and 8 scans for collecting sample spectra. About 20 mg of the ground catalyst was placed in the cell and pretreated at 400 °C for 0.5 h in a flow of Ar (30 mL min^{-1}) to remove water and carbonate in the catalyst. Subsequently, the system was cooled to 30 °C, and the background spectrum was recorded. After the introduction of the gas mixture (1% CO in Ar) for 10 min, the catalyst was purged with Ar for 20 min to remove the physisorbed CO. Then,the cell was sealed and the spectra were collected at 30, 75, and 150 °C. The temperature was controlled with a thermocouple in direct contact with the sample, and circulating water was used to cool the body of the cell.

2.3. Catalytic Testing. The CO oxidation was carried out in a quartz tubular microreactor (i.d. = 6 mm). A 100-mg portion of powdered catalyst was loaded in the reactor, and the reaction temperature was monitored by a thermal couple placed in the middle of the catalyst bed. The catalyst was used without any pretreatment. A reaction mixture of 1% CO, 1% O_2 in N_2 was introduced into the catalyst bed, and the total gas flow rate was 16 mL min^{-1}, corresponding to a space velocity (S.V.) of 9600 mL g^{-1} h^{-1}. Each analysis was taken after the reaction was held for 0.5 h. The inlet and outlet gas mixtures were analyzed on an Agilent 6850 gas chromatograph equipped with a TCD detector attached with a HP PLOT column (30 m × 0.32 mm × 12.0 μm).

3. Results

3.1. Structure Characterization. The surface areas of the synthesized $Ce_{0.9}Pr_{0.1}O_{2-\delta}$, $Ce_{0.95}Cu_{0.05}O_{2-\delta}$, $Ce_{0.9}Pr_{0.05}Cu_{0.05}O_{2-\delta}$, and CeO_2 samples were 30, 2, 8, and 17 m^2 g^{-1}, respectively, determined by N_2 sorption. The decline in surface area for the Cu-containing samples was probably due to the sintering of CuO particles during the high-temperature calcination. Cu dispersions for the $Ce_{0.95}Cu_{0.05}O_{2-\delta}$, $Ce_{0.9}Pr_{0.05}Cu_{0.05}O_{2-\delta}$

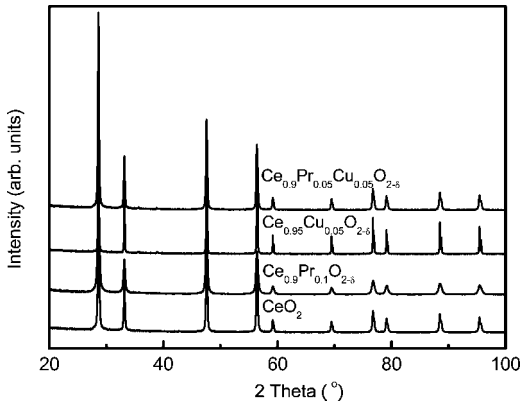

Figure 1. XRD patterns of $Ce_{0.95}Cu_{0.05}O_{2-\delta}$, $Ce_{0.9}Pr_{0.1}O_{2-\delta}$, $Ce_{0.9}Pr_{0.05}Cu_{0.05}O_{2-\delta}$, and CeO_2 samples.

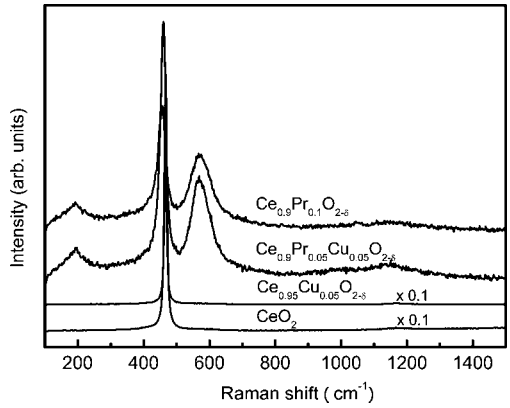

Figure 2. Raman spectra of $Ce_{0.95}Cu_{0.05}O_{2-\delta}$, $Ce_{0.9}Pr_{0.1}O_{2-\delta}$, $Ce_{0.9}Pr_{0.05}Cu_{0.05}O_{2-\delta}$, and CeO_2 samples.

samples are 29.3 and 40.7%, respectively, according to the N_2O chemisorption results.

Figure 1 shows the XRD patterns of the $Ce_{0.9}Pr_{0.1}O_{2-\delta}$, $Ce_{0.95}Cu_{0.05}O_{2-\delta}$, $Ce_{0.9}Pr_{0.05}Cu_{0.05}O_{2-\delta}$, and CeO_2 samples. It was found that only diffraction peaks due to the cubic CeO_2 phase, and no diffraction peaks due to the CuO or Pr_6O_{11} phases, were observed. The lattice parameters of the samples analyzed by the Jade 6.5 software were 0.5413, 0.5412, 0.5413, and 0.5413 nm for the CeO_2, $Ce_{0.9}Pr_{0.1}O_{2-\delta}$, $Ce_{0.95}Cu_{0.05}O_{2-\delta}$, and $Ce_{0.9}Pr_{0.05}Cu_{0.05}O_{2-\delta}$ catalysts, respectively, indicating that there was no obvious change in the lattice parameters after the Cu or/and Pr ions were introduced. The crystallite sizes of the $Ce_{0.9}Pr_{0.1}O_{2-\delta}$, $Ce_{0.95}Cu_{0.05}O_{2-\delta}$, $Ce_{0.9}Pr_{0.05}Cu_{0.05}O_{2-\delta}$, and CeO_2 samples were 24.5, 100, 49.6, and 48.8 nm, respectively, determined by Rietveld refinement.

The XRD technique reflects more information in the bulk and is generally insensitive to the components with high dispersion or low concentration, whereas Raman spectroscopy provides more information on the surface of the catalyst. Figure 2 shows the Raman spectra of the samples. It can be seen that both the pure CeO_2 and the $Ce_{0.95}Cu_{0.05}O_{2-\delta}$ mixed oxide show a Raman band at 465 cm^{-1}, which, according to McBride,[30] was ascribed to the $F_{2\,g}$ vibration mode of fluorite structure of pure CeO_2. For the $Ce_{0.9}Pr_{0.1}O_{2-\delta}$ and the $Ce_{0.9}Pr_{0.05}Cu_{0.05}O_{2-\delta}$ samples, the band ascribed to the $F_{2\,g}$ mode of CeO_2 shifted to lower frequency at about 460 cm^{-1}, which was due to the fact that the sample in the current study is a nanosized material.[31] Apart from the band at 460 cm^{-1}, three bands were observed at 195, 570, and 1150 cm^{-1} for the $Ce_{0.9}Pr_{0.1}O_{2-\delta}$ and the $Ce_{0.9}Pr_{0.05}Cu_{0.05}O_{2-\delta}$ samples. The bands at 195 and 570 cm^{-1} were ascribed to oxygen vacancies according to McBride et al.,[32] whereas the weak band at 1150 cm^{-1} was ascribed to primary A_{1g} asymmetry of CeO_2.[29] The appearance of the bands at 195 and 570 cm^{-1} indicated that the formation of solid solution was beneficial to the formation of oxygen vacancies, which also further illustrated that the Ce—Pr—O solid solution was formed when Pr ions were introduced to the CeO_2 lattice. However, the band at 570 cm^{-1} ascribed to oxygen vacancies was not observed in the $Ce_{0.95}Cu_{0.05}O_{2-\delta}$ sample.

The peak areas of the bands at 460 and 570 cm^{-1} were calculated based on the results shown in Figure 2, which were denoted as A_{460} and A_{570}, respectively. The ratio of A_{570}/A_{460} reflects the concentration of oxygen vacancies in the solid solution.[28] The A_{570}/A_{460} values for the $Ce_{0.9}Pr_{0.1}O_{2-\delta}$ and the $Ce_{0.9}Pr_{0.05}Cu_{0.05}O_{2-\delta}$ samples were 1.50 and 1.10, respectively.

3.2. In Situ Raman and DRIFTS Characterizations. Figure 3 shows the in situ Raman spectra of the $Ce_{0.9}Pr_{0.1}O_{2-\delta}$ and the $Ce_{0.9}Pr_{0.05}Cu_{0.05}O_{2-\delta}$ samples under different atmospheres. Four Raman bands at 195, 460, 570, and 1150 cm^{-1} were observed for both the $Ce_{0.9}Pr_{0.1}O_{2-\delta}$ and the $Ce_{0.9}Pr_{0.05}Cu_{0.05}O_{2-\delta}$ samples under the O_2—N_2, CO—O_2—N_2 and CO—N_2 mixtures. For the $Ce_{0.9}Pr_{0.1}O_{2-\delta}$ catalyst in O_2-containing atmospheres of O_2—N_2 and CO—O_2—N_2, the band at 570 cm^{-1} became broader and its intensity decreased with increasing temperature; but it was fully recovered after the sample was cooled to room temperature. Also, the band at 460 cm^{-1} shifted to a lower frequency with increasing temperature, and it returned to its initial position after the sample was cooled to room temperature. However, the Raman spectra in the reducing atmosphere of CO—N_2 were very different from that in the O_2—N_2 or the O_2—CO—N_2 mixture: the intensity of the band at 570 cm^{-1} decreased with increasing temperature, while its position did not change below 300 °C, but it shifted to lower frequency at about 540 cm^{-1} when the temperature was higher than 300 °C with little change in its intensity in the temperature range of 300−500 °C. When the sample was cooled to room temperature and O_2 was introduced, the position and intensity of the band due to oxygen vacancies also reverted completely. The trend of the change in position and intensity of the feature bands for the $Ce_{0.9}Pr_{0.05}Cu_{0.05}O_{2-\delta}$ catalyst was similar to that for the $Ce_{0.9}Pr_{0.1}O_{2-\delta}$ catalyst.

The peak areas of the bands at 460 (A_{460}) and 570 cm^{-1} (A_{570}) were calculated based on the in situ Raman results in Figure 3. Figure 4 shows the relationship between A_{570}/A_{460} and temperature under different atmospheres for the $Ce_{0.9}Pr_{0.1}O_{2-\delta}$ and the $Ce_{0.9}Pr_{0.05}Cu_{0.05}O_{2-\delta}$ catalysts. The changing trends of the A_{570}/A_{460} value for the two samples were very similar. The A_{570}/A_{460} value decreased with increasing temperature under all atmospheres. Moreover, the value is slightly higher for the sample in O_2—N_2 at each temperature point than that in CO—O_2—N_2, with similar slopes of decline. Whereas for the samples in CO—N_2, the A_{570}/A_{460} value was much lower than that in O_2—N_2 or O_2—CO—N_2, with a much faster decline. After all, when the samples were cooled to room temperature, the A_{570}/A_{460} value completely recovered.

Figure 5 shows the DRIFT spectra of CO chemisorption over the catalysts at different temperatures. All of the catalysts show peaks at 1000−1600 cm^{-1} (not shown), which are characteristic of carbonate or carboxylate adsorbed on the catalyst surface.[15] In the region from 1800 to 2400 cm^{-1}, an adsorption peak at 2110 cm^{-1} was observed for the Cu-containing catalysts ($Ce_{0.95}Cu_{0.05}O_{2-\delta}$ and $Ce_{0.9}Pr_{0.05}Cu_{0.05}O_{2-\delta}$), which was attributed to chemisorbed CO,[15] although this peak is less intense for the $Ce_{0.95}Cu_{0.05}O_{2-\delta}$ compared to the $Ce_{0.9}Pr_{0.05}Cu_{0.05}O_{2-\delta}$. When the temperature increased to 75 °C, the peak at 2110 cm^{-1}

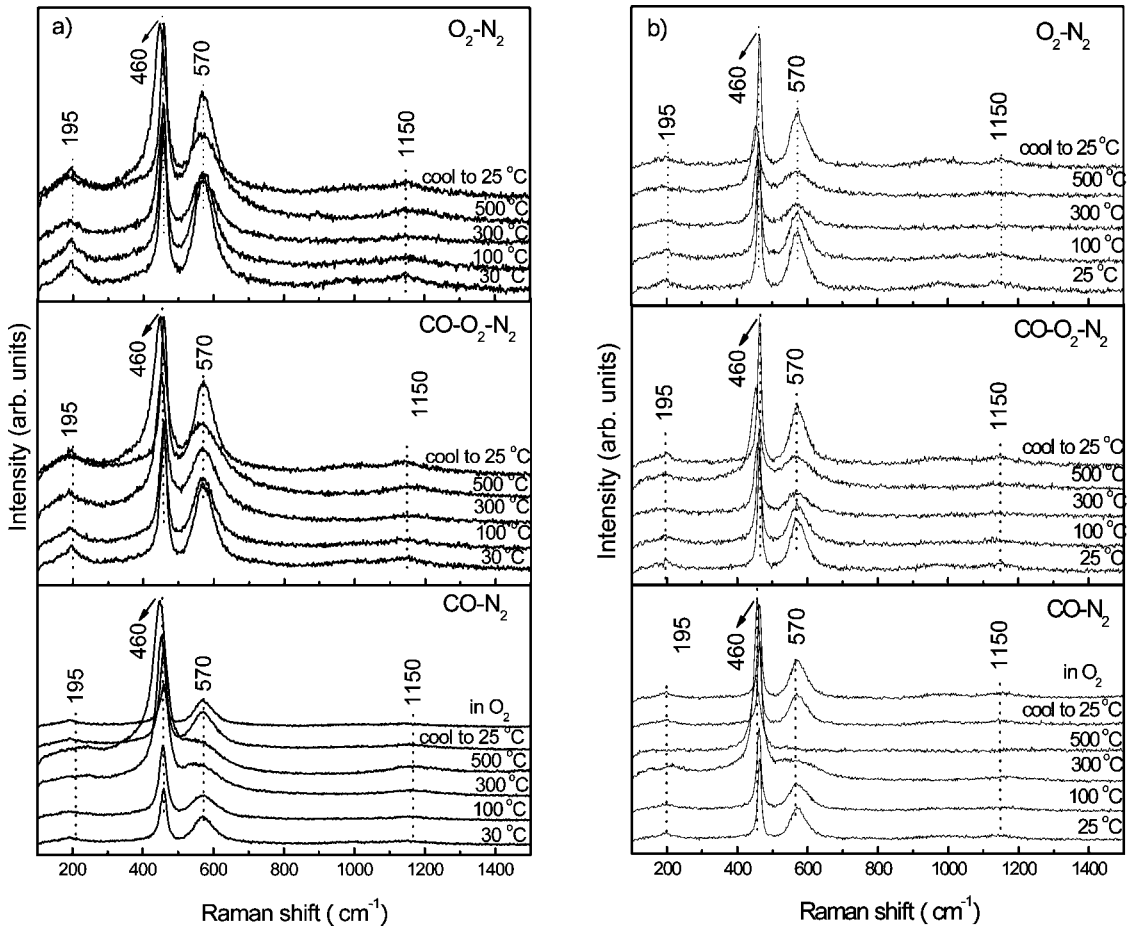

Figure 3. In situ Raman spectra of (a) $Ce_{0.9}Pr_{0.1}O_{2-\delta}$ and (b) $Ce_{0.9}Pr_{0.05}Cu_{0.05}O_{2-\delta}$ samples under different atmospheres.

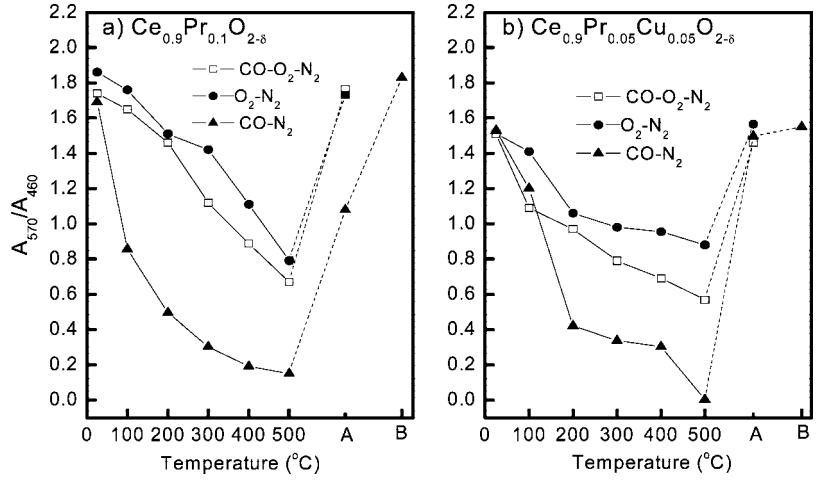

Figure 4. Relationship between A_{570}/A_{460} and temperature under different atmospheres for (a) $Ce_{0.9}Pr_{0.1}O_{2-\delta}$ and (b) $Ce_{0.9}Pr_{0.05}Cu_{0.05}O_{2-\delta}$ samples.

disappeared for the $Ce_{0.9}Pr_{0.05}Cu_{0.05}O_{2-\delta}$, while it remained for the $Ce_{0.95}Cu_{0.05}O_{2-\delta}$, until the temperature further increased to 150 °C.

3.3. Catalytic Test of CO Oxidation. Figure 6 shows CO oxidation over the $Ce_{0.95}Cu_{0.05}O_{2-\delta}$, $Ce_{0.9}Pr_{0.1}O_{2-\delta}$, $Ce_{0.9}Pr_{0.05}$-$Cu_{0.05}O_{2-\delta}$, and CeO_2 catalysts. It can be seen that the T_{90} (the temperature at which the CO conversion is 90%) for the CeO_2, $Ce_{0.9}Pr_{0.1}O_{2-\delta}$, $Ce_{0.95}Cu_{0.05}O_{2-\delta}$, and $Ce_{0.9}Pr_{0.05}Cu_{0.05}O_{2-\delta}$ catalysts were 380, 280, 200, and 120 °C, respectively. Compared to the pure CeO_2, the $Ce_{0.9}Pr_{0.1}O_{2-\delta}$ catalyst was more active, while the $Ce_{0.95}Cu_{0.05}O_{2-\delta}$ catalyst was more active than the $Ce_{0.9}$-$Pr_{0.1}O_{2-\delta}$ catalyst. With both Pr and Cu introduced in the catalyst, the $Ce_{0.9}Pr_{0.05}Cu_{0.05}O_{2-\delta}$ catalyst showed the highest activity, strongly indicating the synergistic effect of Cu and Pr on the promotion of reactivity.

4. Discussion

4.1. Structural Properties of the CeO_2-Based Samples. In this work, several CeO_2-based mixed-oxide catalysts were prepared by a sol−gel method. The structural properties of these samples were characterized using XRD and Raman techniques. From the XRD results (Figure 1), it is obvious that CeO_2 solid solution was formed as the diffraction peaks match the cubic CeO_2 phase without any observed diffraction peaks due to the

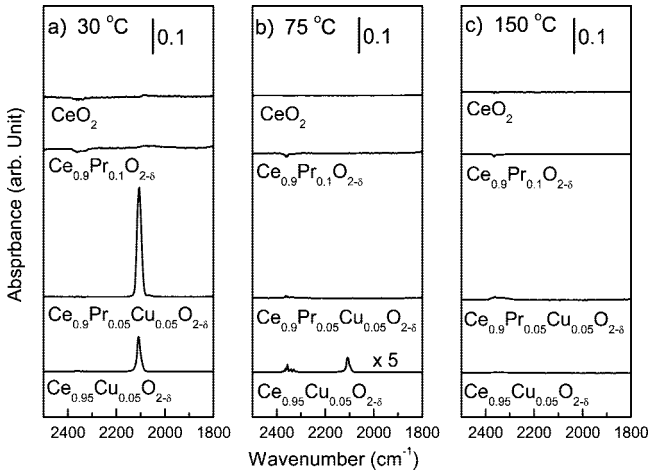

Figure 5. In situ DRIFT spectra for CO chemisorption on CeO_2, $Ce_{0.9}Pr_{0.1}O_{2-\delta}$, $Ce_{0.95}Cu_{0.05}O_{2-\delta}$, and $Ce_{0.9}Pr_{0.05}Cu_{0.05}O_{2-\delta}$ at (a) 30 °C, (b) 75 °C, and (c) 150 °C.

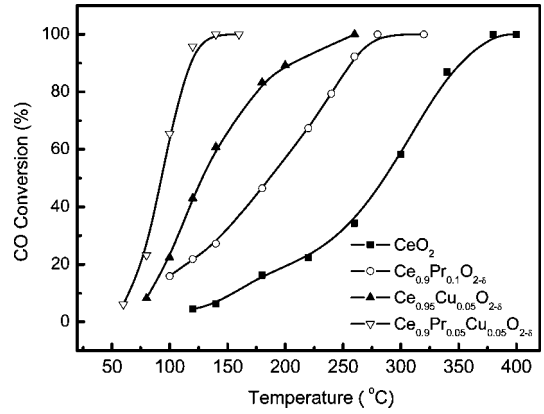

Figure 6. CO oxidation over $Ce_{0.95}Cu_{0.05}O_{2-\delta}$, $Ce_{0.9}Pr_{0.1}O_{2-\delta}$, $Ce_{0.9}Pr_{0.05}Cu_{0.05}O_{2-\delta}$, and CeO_2 samples.

Pr_6O_{11} or CuO phase. Furthermore, the lattice parameters of these samples are close to each other. For the $Ce_{0.9}Pr_{0.1}O_{2-\delta}$ sample, the lattice parameter (0.5412 nm) is very close to that of CeO_2 (0.5413 nm), which is because the radius of Pr^{3+} ion (0.096 nm) is almost identical to that of Ce^{4+} ion (0.097 nm), thus it changed slightly when Ce^{4+} ion was partially substituted by Pr^{3+} ion. For the Cu-containing samples, as the radius of Cu^{2+} ion (0.072 nm) is much smaller than that of Ce^{4+} ion (0.097 nm), the changes in the lattice parameters are supposed to be more significant than that of the $Ce_{0.9}Pr_{0.1}O_{2-\delta}$ sample if Ce^{4+} was substituted by Cu^{2+}. However, the lattice parameter hardly changes after the Cu ions were introduced. This is likely because very few Cu ions penetrated into the CeO_2 lattice. Nevertheless, no diffraction peaks of CuO species were detected by XRD, which is probably due to the fact that the CuO species are highly dispersed on the surface of catalyst or the CuO content was below the detection limit of XRD.

The samples were also characterized with Raman spectroscopy in order to obtain surface information. Compared to the pure CeO_2, the Pr-doped mixed oxides exhibit much higher concentrations of oxygen vacancies, which is consistent with a previous report.[28] The ratio of A_{570}/A_{460} is higher on the $Ce_{0.9}Pr_{0.1}O_{2-\delta}$ sample ($A_{570}/A_{460} = 1.50$) than that on the $Ce_{0.9}Pr_{0.05}Cu_{0.05}O_{2-\delta}$ sample ($A_{570}/A_{460} = 1.10$), which could be explained by the higher Pr content in the former sample because as pointed out in our previous paper that the A_{570}/A_{460} value is proportional to the surface Pr content in the Ce—Pr—O mixed oxide.[28]

4.2. Roles of Oxygen Vacancies and CuO Species in the CO Oxidation. The CO oxidation over Cu—Ce—O catalysts has been extensively investigated.[11,16,18] It is well recognized that both the oxygen vacancies provided by the support and the chemisorption of CO on CuO species are very important to the reaction. It was pointed out that the adsorption of oxygen on the surface of some oxide such as CeO_2 leads to the formation of O_2^- anion radicals.[21,33] Bozo et al.[20] proposed that the presence of oxygen vacancies appeared to be an important role in the catalytic activity due to the fact that they provide sites for oxygen activation by formation of superoxide (O_2^-), which was considered as the intermediate species in the oxidative reactions accruing on the catalysts surface. Lunina et al.[34] studied the formation of O_2^- anion radicals on the surface of CeO_2—ZrO_2 and Y_2O_3—CeO_2—ZrO_2 solid solutions, and found that the introduction of Y_2O_3 into the CeO_2—ZrO_2 solid solution led to the formation of more reactive O_2^- anion radicals. In the current study, it was found that the $Ce_{0.9}Pr_{0.1}O_{2-\delta}$ is more active than the pure CeO_2 (Figure 6), which also can be possibly related to a higher concentration of oxygen vacancies in the $Ce_{0.9}Pr_{0.1}O_{2-\delta}$ (Figure 2), due to the partial replacement of Ce^{4+} by Pr^{3+}/Pr^{4+} in the CeO_2 matrix. However, it should be noted that the above conclusion was obtained on the fresh catalyst, and the surface properties including oxygen vacancies might change during the reaction process because of the presence of the reducing agent CO in the reaction mixture, the in situ characterization is therefore very necessary. In this work, the in situ Raman experiments were carried out in order to obtain surface information during the reaction process (Figure 3). It was found that the changing trends of the two catalysts are similar in the O_2-containing atmospheres, while it is very different in the reducing atmosphere of CO—N_2. Also, the ratio of A_{570}/A_{460} declines along with increasing temperature, with a much steeper slope in CO—N_2 than in O_2—N_2 or CO—O_2—N_2 (Figure 4). This is related to the structural change in the surface, mainly due to the reduction of Pr^{4+} to Pr^{3+}, as discussed in our previous work.[28] In the O_2-containing gases, the decline of the A_{570}/A_{460} is due to the migration of surface Pr to bulk in the heating process, and the recovery of the value is due to the fast redistribution of Pr in the catalyst. However, the decline of the A_{570}/A_{460} value in CO—N_2 mixture is due to the simultaneous influences of migration of surface Pr and the reduction of Pr^{4+} to Pr^{3+} by the reducing agent.[28] The comparison of the A_{570}/A_{460} value at each temperature between the oxidizing gases and the reducing gas indicates that despite the presence of CO in the mixture of CO—O_2—N_2, the catalyst surface remains oxidized during the reaction and a high concentration of oxygen vacancies are maintained in the reaction process, which is beneficial to the reactivity of the Pr or Pr-/Cu-doped CeO_2 mixed oxide.

In this work, it was also found that the $Ce_{0.9}Pr_{0.05}Cu_{0.05}O_{2-\delta}$ and $Ce_{0.95}Cu_{0.05}O_{2-\delta}$ catalysts are more active than the $Ce_{0.9}Pr_{0.1}O_{2-\delta}$ catalyst, suggesting the positive role of CuO species in the reaction. The role of CuO species in CO oxidation over CuO—CeO_2 catalysts has been systematically studied by the group of Martínez-Arias[17,35] and others.[11,12] In general, CuO species provide chemisorption sites for CO at the interfacial location of CuO—CeO_2. Martínez-Arias et al.[36] prepared a series of CuO—CeO_2 catalysts and found that the CO oxidation activity is proportional to the intensity of the Cu+ carbonyl band, and they concluded that the level of reduction of Cu^{2+} in the catalyst is related to the amount of sites available for the chemisorbed CO to react with active oxygen provided by the CeO_2 support and close the catalytic cycle.

SCHEME 1: Scheme of CO Oxidation over $Ce_{0.9}Pr_{0.05}Cu_{0.05}O_{2-\delta}$ Oxide

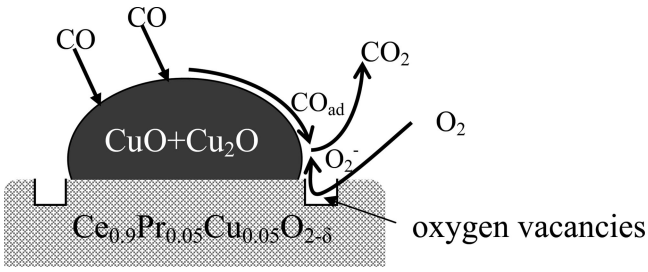

In the present work, it could be observed from Figure 5 that for the Cu-containing samples ($Ce_{0.95}Cu_{0.05}O_{2-\delta}$ and $Ce_{0.9}Pr_{0.05}Cu_{0.05}O_{2-\delta}$), the band at 2110 cm^{-1} corresponds to Cu^+ carbonyl (Cu^+—CO) was found. It was due to the Cu^{2+}/Cu^{1+} redox couple located at the interfacial position of the dispersed CuO species and the CeO_2 support.[15] This suggests that the existence of Cu^+ ions provides sites for the CO chemisorption. However, the CO adsorption peak cannot be observed in the samples without Cu ions ($Ce_{0.9}Pr_{0.1}O_{2-\delta}$ and CeO_2), which accounts for the suppressed activities obtained on these catalysts. Furthermore, the intensity of this Cu^+ carbonyl band is much higher on the $Ce_{0.9}Pr_{0.05}Cu_{0.05}O_{2-\delta}$ catalyst than that on the $Ce_{0.95}Cu_{0.05}O_{2-\delta}$, which is possibly due to the higher Cu dispersion in the $Ce_{0.9}Pr_{0.05}Cu_{0.05}O_{2-\delta}$ catalyst compared to the $Ce_{0.95}Cu_{0.05}O_{2-\delta}$, as evidenced by N_2O chemisorption. Moreover, the feature of Cu^+ carbonyl disappeared at 75 °C for the $Ce_{0.9}Pr_{0.05}Cu_{0.05}O_{2-\delta}$ sample, while for the $Ce_{0.95}Cu_{0.05}O_{2-\delta}$ sample, the feature still remains at 75 °C, and it completely disappeared until 150 °C. The difference in decomposition of Cu^+-carbonyl species between the $Ce_{0.9}Pr_{0.05}Cu_{0.05}O_{2-\delta}$ and the $Ce_{0.95}Cu_{0.05}O_{2-\delta}$ samples implies that the oxygen vacancies on the surface of the $Ce_{0.9}Pr_{0.05}Cu_{0.05}O_{2-\delta}$ sample were involved in the oxidation of the chemisorbed CO species, which enhances the reactivity. Interestingly, when one compares the $Ce_{0.95}Cu_{0.05}O_{2-\delta}$ with the $Ce_{0.9}Pr_{0.1}O_{2-\delta}$, it was found that although the concentration of the oxygen vacancies is high in the $Ce_{0.9}Pr_{0.1}O_{2-\delta}$, the $Ce_{0.95}Cu_{0.05}O_{2-\delta}$ catalyst is more active than the $Ce_{0.9}Pr_{0.1}O_{2-\delta}$ catalyst, implying that the role of Cu^+ (for CO chemisorption) is more pronounced than that of the oxygen vacancies in the CO oxidation.

Since the reactivity of CO oxidation is dependent on the chemisorbed CO and the active oxygen, higher concentrations of these intermediates on the catalyst surface can certainly enhance the reactivity, as evidenced in the current study. The $Ce_{0.9}Pr_{0.05}Cu_{0.05}O_{2-\delta}$ catalyst shows the highest reactivity compared to others, due to its high density of oxygen vacancies and chemisorption sites for CO. Such a synergistic effect could be explained by the redox property at the interface of CuO and CeO_2, as illustrated in Scheme 1. We propose that the reaction pathway for CO oxidation consists of three steps: (1) O_2 and CO chemisorption on the oxygen vacancies and Cu^+ ions in the catalyst surface, respectively; (2) the adsorbed O_2 is activated to O_2^- anion radicals rapidly by oxygen vacancies; and (3) the chemisorbed CO migrates to the periphery of the CuO—CeO_2 interface and reacts with the activated O_2^- and generates CO_2,[37] thus leaving empty the Cu^+ site and oxygen vacancies and closing the catalytic cycle.

5. Conclusions

In this work, several CeO_2-based mixed oxides were prepared and characterized with various techniques. The Raman results show that an increase in oxygen vacancy concentration due to the Pr doping in the catalyst, while the in situ DRIFTS results reveal the chemisorption of CO on Cu^+ ions on the catalyst surface. The in situ Raman spectra indicate that the surfaces of $Ce_{0.9}Pr_{0.1}O_{2-\delta}$ and $Ce_{0.9}Pr_{0.05}Cu_{0.05}O_{2-\delta}$ samples are close to oxidation state, despite of the presence of CO in the reaction mixture. When these catalysts were employed for catalytic CO oxidation, it was found that the Cu- and Pr-doped catalysts show the highest activity. The enhancement in reactivity is strongly related to the higher concentrations of oxygen vacancies on the surface of the support and the chemisorbed CO on the Cu^+ sites. More importantly, these findings demonstrate a promising approach that remarkably enhanced reactivity could be achieved for CO oxidation over CuO—CeO_2 catalysts, if the CeO_2 based support with more oxygen vacancies could be synthesized.

Acknowledgment. This work is financially supported by the National Science Foundation of China (Grant No. 20473075) and by the Science and Technology Foundation of Zhejiang Province (Grant No. 2007F70024). We would like to express our thanks to Mr. Zhi-ming Liu from Dalian Institute of Chemical Physics (DICP) for assistance with the in situ DRIFTS experiments.

References and Notes

(1) Schryer, D. R.; Upchurch, B. T.; Sidney, B. D.; Brown, K. G.; Hoflund, G. B.; Herz, R. K. *J. Catal.* **1991**, *130*, 314.
(2) Yuan, Y. Z.; Kozlova, A. P.; Asakura, K.; Wan, H. L.; Tsai, K.; Iwasawa, Y. *J. Catal.* **1997**, *170*, 191.
(3) Bollinger, M. A.; Vannice, M. A. *Appl. Catal., B* **1996**, *8*, 417.
(4) Chen, M. S.; Goodman, D. W. *Science* **2004**, *306*, 252.
(5) Park, E. D.; Lee, J. S. *J. Catal.* **1999**, *186*, 1.
(6) Wolf, A.; Schuth, F. *Appl. Catal., A* **2002**, *226*, 1.
(7) Engel, T.; Ertl, G. *Adv. Catal.* **1979**, *28*, 1.
(8) Huang, T. J.; Yu, T. C.; Chang, S. H. *Appl. Catal.* **1989**, *52*, 157.
(9) Luo, M. F.; Zhong, Y. J.; Yuan, X. X.; Zheng, X. M. *Appl. Catal., A* **1997**, *162*, 121.
(10) Luo, M. F.; Song, Y. P.; Lu, J. Q.; Wang, X. Y.; Pu, Z. Y. *J. Phys. Chem. C* **2007**, *111*, 12686.
(11) Liu, W.; Flytzani-Stephanopoulos, M. *J. Catal.* **1995**, *153*, 304.
(12) Liu, W.; Flytzani-Stephanopoulos, M. *J. Catal.* **1995**, *153*, 317.
(13) Liu, W.; Flytzani-Stephanopoulos, M. *Chem. Eng. J.* **1996**, *64*, 283.
(14) Luo, M. F.; Ma, J. M.; Lu, J. Q.; Song, Y. P.; Wang, Y. J. *J. Catal.* **2007**, *246*, 52.
(15) Martínez-Arias, A.; Ferñandez-Garcia, M.; Galvez, O.; Coronado, J. M.; Anderson, J. A.; Conesa, J. C.; Soria, J.; Munuera, G. *J. Catal.* **2000**, *195*, 207.
(16) Martínez-Arias, A.; Hungría, A. B.; Fernández-García, M.; Conesa, J. C.; Munuera, G. *J. Phys. Chem. B.* **2004**, *108*, 17983.
(17) Martínez-Arias, A.; Fernández-García, M.; Hungría, A. B.; Iglesias-Juez, A.; Gálvez, O.; Anderson, J. A.; Conesa, J. C.; Soria, J.; Munuera, G. *J. Catal.* **2003**, *214*, 261.
(18) Tang, X. L.; Zhang, B. C.; Li, Y.; Xu, Y. D.; Xin, Q.; Shen, W. J. *Catal. Today* **2004**, *93*−*95*, 191.
(19) Lin, R.; Luo, M. F.; Zhong, Y. J.; Yan, Z. L.; Liu, G. Y.; Liu, W. P. *Appl. Catal., A* **2003**, *255*, 331.
(20) Bozo, C.; Guilhaume, N.; Herrmann, J. M. *J. Catal.* **2001**, *203*, 393.
(21) Fierro, J. L. G.; Soria, J.; Sanz, J.; Rojo, J. M. *J. Solid State Chem.* **1987**, *66*, 154.
(22) Sayle, T. X. T.; Parker, S. C.; Catlow, C. R. A. *Surf. Sci.* **1994**, *316*, 329.
(23) Sedmak, G.; Hoèevar, S.; Levec, J. *J. Catal.* **2004**, *222*, 87.
(24) Sedmak, G.; Hoèevar, S.; Levec, J. *J. Catal.* **2003**, *213*, 135.
(25) Sedmak, G.; Hoèevar, S.; Levec, J. *Top. Catal.* **2004**, *30*−*31*, 445.
(26) Hartridge, A.; Krishna, M. G.; Bhattacharya, A. K. *Mater. Sci. Eng., B* **1999**, *57*, 173.
(27) Cho, B. K. *J. Catal.* **1991**, *131*, 74.
(28) Pu, Z. Y.; Lu, J. Q.; Luo, M. F.; Xie, Y. L. *J. Phys. Chem. C* **2007**, *111*, 18695.
(29) Velu, S.; Suzuki, K.; Osaki., T. *Catal. Lett.* **1999**, *62*, 159.
(30) Weber, W. H.; Hass, K. C.; McBride, J. R. *Phys. Rev. B* **1993**, *48*, 178.
(31) Spanier, J. E.; Robinson, R. D.; Zhang, F.; Chan, S. W.; Herman, I. P. *Phys. Rev. B* **2001**, *64*, 245407.
(32) McBride, J. R.; Hass, K. C.; Poindexter, B. D.; Weber, W. H. *J. Appl. Phys.* **1994**, *76*, 2435.

(33) Zhang, X. L.; Klabunde, K. J. *Inorg. Chem.* **1992**, *31*, 1706.
(34) Markaryan, G. L.; Ikryannikova, L. N.; Muravieva, G. P.; Turakulova, A. O.; Kostyuk, B. G.; Lunina, E. V.; Lunin, V. V.; Zhilinskaya, E.; Aboukais, A. *Colloids Surf. A* **1999**, *151*, 435.
(35) Gamarra, D.; Munuera, G.; Hungría, A. B.; Fernández-García, M.; Conesa, J. C.; Midgley, P. A.; Wang, X. Q.; Hanson, J. C.; Rodríguez, J. A.; Martínez-Arias, A. *J. Phys. Chem. C* **2007**, *111*, 11026.
(36) Gamarra, D.; Belver, C.; Fernández-García, M.; Martínez-Arías, A. *J. Am. Chem. Soc.* **2007**, *129*, 12064.
(37) Tang, X. L.; Zhang, B. C.; Li, Y.; Xu, Y. D.; Xin, Q.; Shen, W. J. *Appl. Catal., A* **2005**, *288*, 116.

JP805389K